Polarized neutron diffraction and Mössbauer spectral study of short-range magnetic correlations in the ferrimagnetic layered compounds (PPh_4) $[Fe^{II}Fe^{III}(ox)_3]$ and (NBu_4) $[Fe^{II}Fe^{III}(ox)_3]$

Simon G. Carling,[1] Dirk Visser,[2,3,4] Dimitri Hautot,[1] Ian D. Watts,[1] Peter Day,[1] Jürgen Ensling,[5] Phillip Gütlich,[5] Gary J. Long,[6] and Fernande Grandjean[7]

[1]*Royal Institution of Great Britain, London W1S 4BS, United Kingdom*

[2]*Department of Physics, University of Warwick, Coventry CV4 7AL, United Kingdom*

[3]*NWO-EW, ISIS Facility, Rutherford Appleton Laboratory, Chilton, Didcot, OX11 0QX, United Kingdom*

[4]*IRI, TU-Delft, Mekelweg 15, 2629 JB Delft, Netherlands*

[5]*Institut für Anorganische Chemie und Analytische Chemie, J. Gutenberg-Universität Mainz, Staudinger Weg 9, D-55099 Mainz, Germany*

[6]*Department of Chemistry, University of Missouri-Rolla, Rolla, Missouri 65409-0010*

[7]*Institut de Physique, B5, Université de Liège, B-4000 Sart-Tilman, Belgium*

(Received 27 November 2001; revised manuscript received 2 July 2002; published 9 September 2002)

Short-range antiferromagnetic correlations have been studied in the layered compounds (PPh_4) $[Fe^{II}Fe^{III}(ox)_3]$ and (NBu_4) $[Fe^{II}Fe^{III}(ox)_3]$ by neutron polarization analysis and Mössbauer spectroscopy. Polarized neutron diffraction profiles obtained between 2 and 50 K on $(d_{20}\text{-}PPh_4)$ $[Fe^{II}Fe^{III}(ox)_3]$ show no magnetic Bragg scattering; the lack of such scattering indicates the absence of long-range magnetic order. However, a broad asymmetric feature observed at a Q of ca. 0.8 $Å^{-1}$ is attributed to two-dimensional short-range magnetic correlations, which are described by a Warren function. The correlation length is ca. 50 Å between 2 and 30 K and then decreases to ca. 20 Å at 50 K. The Mössbauer spectra of (PPh_4) $[Fe^{II}Fe^{III}(ox)_3]$ and (NBu_4) $[Fe^{II}Fe^{III}(ox)_3]$ have been measured between 1.9 and 293 K and 1.9 and 315 K, respectively, and are very similar. The paramagnetic spectra exhibit both high-spin Fe^{II} and Fe^{III} doublets with relative areas which indicate a 5% and 2% excess, respectively, of Fe^{III}. The coexistence in (PPh_4) $[Fe^{II}Fe^{III}(ox)_3]$ between 10 and 30 K of broad sextets and doublets in the Mössbauer spectra and the paramagnetic scattering observed in the polarized neutron measurements indicate the coexistence of spin-correlated and spin-uncorrelated regions in the layers of this compound. The polarized neutron scattering profiles and the Mössbauer spectra yield the magnetic exchange correlation length and lifetime, respectively, and the combined results are best understood in terms of layers composed of random frozen, but exchange correlated domains of ca. 50 Å diameter at the lowest temperatures, of spin-correlated domains and spin-uncorrelated regions at intermediate temperatures, and of largely spin-uncorrelated regions above the Néel temperature as determined from magnetometry. The similarity of the Mössbauer spectra of (PPh_4) $[Fe^{II}Fe^{III}(ox)_3]$ and (NBu_4) $[Fe^{II}Fe^{III}(ox)_3]$ leads to the conclusion that similar magnetic exchange correlations are present in the latter compound.

DOI: 10.1103/PhysRevB.66.104407 PACS number(s): 75.25.+z, 76.80.+y, 75.30.Kz

I. INTRODUCTION

The layered molecular-based ferromagnets and ferrimagnets (A) $[M^{II}M^{III}(ox)_3]$, where A is an organic cation, M^{II} and M^{III} are $3d$ ions, and (ox) is the oxalate anion, $C_2O_4{}^{2-}$, are attractive systems in which to observe the establishment of magnetic correlations in two-dimensional honeycomb lattices, and as such they have been the subject of numerous studies.[1–6] In these insulating materials, the M^{II} and M^{III} cations are disposed in an alternating honeycomb array, bridged by oxalates so that each metal has a trigonally distorted octahedral environment, and the A cations lie in between the metal-oxalate layers, often with one or more side chains penetrating into the hexagonal cavities between the oxalates. Among the many compounds of this type, those containing Fe^{II} and Fe^{III} have proved particularly fascinating. Both metal ions are in the high-spin state and the near-neighbor magnetic exchange is antiferromagnetic. For many A, the bulk magnetization of the resulting compounds resembles that of a Néel class-N ferrimagnet[7] with a compensation temperature and a negative magnetization at low temperature in small applied field. In contrast, where the A cation is tetraphenyl-phosphonium or tetraphenyl-arsonium, the bulk magnetization resembles[7] Néel's class Q with monotonically increasing magnetization below the apparent ordering temperature T_N and no compensation behavior. Examples of the magnetization of each class of materials can be found in Fig. 1, which shows recent magnetization measurements on compounds whose behavior we have reported earlier.[6] Néel ascribed such differences in bulk magnetization to different ordering rates of the two sublattices in a ferrimagnet. Recent magnetometry and Monte Carlo studies[8] on compounds doped with diamagnetic ions suggest that the apparently type-N behavior is inhibited and then destroyed by increasing deficiency on the divalent magnetic sublattice. Unpolarized powder neutron diffraction measurements performed on $(d_{20}\text{-}PPh_4)$ $[Fe^{II}Fe^{III}(ox)_3]$ (Ref. 9) showed a broad magnetic feature below 35 K; unfortunately this feature overlapped with a strong nuclear Bragg peak and could not be thoroughly analyzed. The temperature dependence of the intensity of this feature resembled that expected for a sublattice magnetization.

In this paper we present detailed Mössbauer spectral data measured between 295 and 1.9 K for one example of each type, $A^+ = PPh_4^+$ [type *Q*, $PPh_4^+ = P(C_6H_5)_4^+$] and $A^+ = NBu_4^+$ [type *N*, $NBu_4^+ = N(n\text{-}C_4H_9)_4^+$] to probe the reasons for the difference in the ordering process in the two types. This study is complemented by neutron polarization analysis measurements on $(d_{20}\text{-}PPh_4)$ $[Fe^{II}Fe^{III}(ox)_3]$ which directly monitor the buildup of short-range exchange correlations above T_c and the coexistence of correlated and paramagnetic regions below T_c. The neutron measurements of the spatial magnetic exchange correlation, with a time scale of $\sim 10^{-11}$ s, serve to supplement the time-dependent magnetic exchange correlation observed in the Mössbauer results, for which the time scale is $\sim 10^{-8}$ s. Preliminary polarization analysis measurements on $(d_{20}\text{-}PPh_4)$ $[Fe^{II}Fe^{III}(ox)_3]$ at 5 K have already been reported.[10]

Although there have been no detailed reports on the Mössbauer spectral properties of (PPh_4) $[Fe_2(ox)_3]$, the spectral properties of (NBu_4) $[Fe_2(ox)_3]$ as well as of the related (NBu_4) $[M^{II}M^{III}(ox)_3]$ compounds have been studied[1,3,5,11–15,17] in detail (Table I). There is good agreement in both the iron(II) and iron(III) hyperfine parameters for the compounds in the paramagnetic state. Below the magnetic ordering temperature, the agreement is also good for the iron(II) site and most authors report a quadrupole interaction of ca. 1.8 mm/s and negative V_{zz} and a surprisingly small hyperfine field of ca. 35–52 kOe for this site. In contrast, for the iron(III) site there are reports of both positive and negative quadrupole interactions of ca. 0.60 mm/s and both positive and negative signs of V_{zz}, although the hyperfine fields are typical of iron(III): the angle θ between this field and the principal axis of the electric field gradient V_{zz} has been reported to have both large and/or small values. These trends are further complemented by studies[14,15] of mixed-metal complexes, such as (NBu_4) $[(Fe_xMn_{1-x})^{II}Cr^{III}(ox)_3]$, (NBu_4) $[(Fe_xNi_{1-x})^{II}Fe^{III}(ox)_3]$, and (NBu_4) $[Mn^{II}(Fe_xCr_{1-x})^{III}(ox)_3]$, in which two different metals of the same oxidation state occupy the same site.

There have been fewer Mössbauer spectral studies with other *A* cations, but Iijima and Mizutani[13] have studied (NBu_4) $[Fe^{II}Fe^{III}(ox)_3]$, $(Nn\text{-propyl}_4)$ $[Fe^{II}Fe^{III}(ox)_3]$, $(Nn\text{-propyl}_4)$ $[Fe^{II}Cr^{III}(ox)_3]$, and $(Nn\text{-propyl}_4)$ $[Mn^{II}Cr^{III}(ox)_3]$ in some detail, the latter of which contains small amounts of iron-57 on the Mn^{II} site and Ovanesyan *et al.*[17] and Bottyán *et al.*[18] have studied $(Nn\text{-pentyl}_4)$ $[Mn^{II}Fe^{III}(ox)_3]$ and $(Nn\text{-pentyl}_4)$ $[Fe^{II}Fe^{III}(ox)_3]$. Finally, the very unusual bulky cations $[Co^{III}(Me_5Cp)_2]^+$ and $[Fe^{III}(Me_5Cp)_2]^+$, which form layered oxalate compounds $[M^{III}(Me_5Cp)_2]$ $[M^{II}M^{III}(ox)_3]$, have been studied by Coronado *et al.*[19] The spectra of many of these compounds will be discussed below as is appropriate.

In order to better understand the complex but virtually unstudied Mössbauer spectral properties of (PPh_4) $[Fe_2(ox)_3]$, we have carried out a parallel study of (NBu_4) $[Fe_2(ox)_3]$, which has proved extremely valuable in understanding the more complex spectra of (PPh_4) $[Fe_2(ox)_3]$. The results of both of these studies are reported and compared herein.

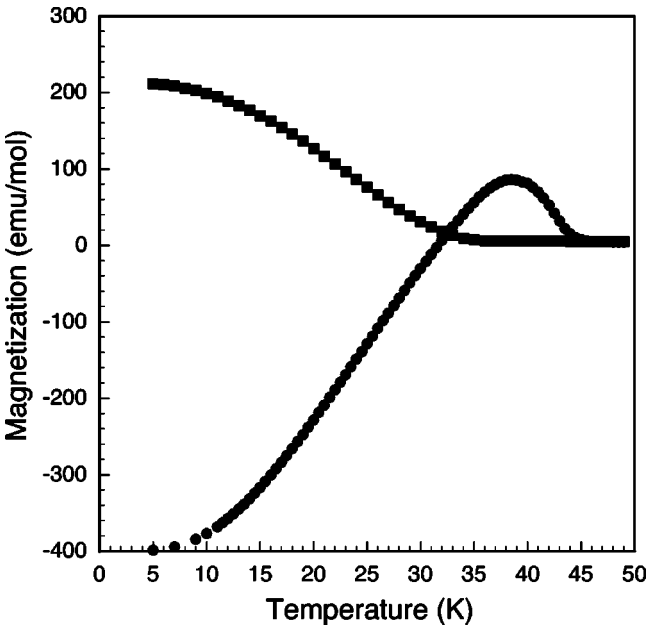

FIG. 1. The temperature dependence of the field-cooled magnetization of $(PPh_4)[Fe_2(ox)_3]$ (■) and $(NBu_4)[Fe_2(ox)_3]$ (●) measured in an applied field of 100 Oe.

II. EXPERIMENT

A. Preparation

The $(d_{20}\text{-}PPh_4)$ $[Fe^{II}Fe^{III}(ox)_3]$ and (NBu_4) $[Fe^{II}Fe^{III}(ox)_3]$ samples were prepared as reported earlier.[6,9] One of the $(d_{20}\text{-}PPh_4)$ $[Fe^{II}Fe^{III}(ox)_3]$ samples was the same as that used in an earlier unpolarized neutron diffraction study.[9] Earlier chemical analysis[20,21] of related (*A*) $[Fe^{II}Fe^{III}(ox)_3]$ compounds have shown a ca. 1%–7% deficiency of iron cations relative to the number of oxalate anions. Because of the extremely high cost of the $(d_{20}\text{-}PPh_4)^+$ cation, no chemical analysis of $(d_{20}\text{-}PPh_4)$ $[Fe^{II}Fe^{III}(ox)_3]$ was performed, but as discussed below, the Mössbauer spectra show a 5% deficiency in iron(II) content relative to the total iron content. This deficiency no doubt results in iron(II) vacancies in the honeycomb lattice, which may be occupied by simple H_3O^+ cations because the complex is made in acidic solution.

B. Magnetization

dc bulk magnetization measurements were performed using a Quantum Design MPMS7 superconducting quantum interference device (SQUID) magnetometer. Samples were accurately weighed to a precision of ± 1 μg and loaded in gelatine capsules which were then mounted in a plastic drinking straw. Magnetization was measured as a function of temperature between 5 and 50 K in an applied field of 100 Oe. The measured data were corrected for diamagnetic contributions using Pascal's constants. Figure 1 shows the magnetizations of $(d_{20}\text{-}PPh_4)$ $[Fe^{II}Fe^{III}(ox)_3]$ and (NBu_4) $[Fe^{II}Fe^{III}(ox)_3]$ as a function of temperature.

C. Neutron diffraction

Polarized neutron diffraction experiments were performed on the diffuse scattering spectrometer D7 at the Institut

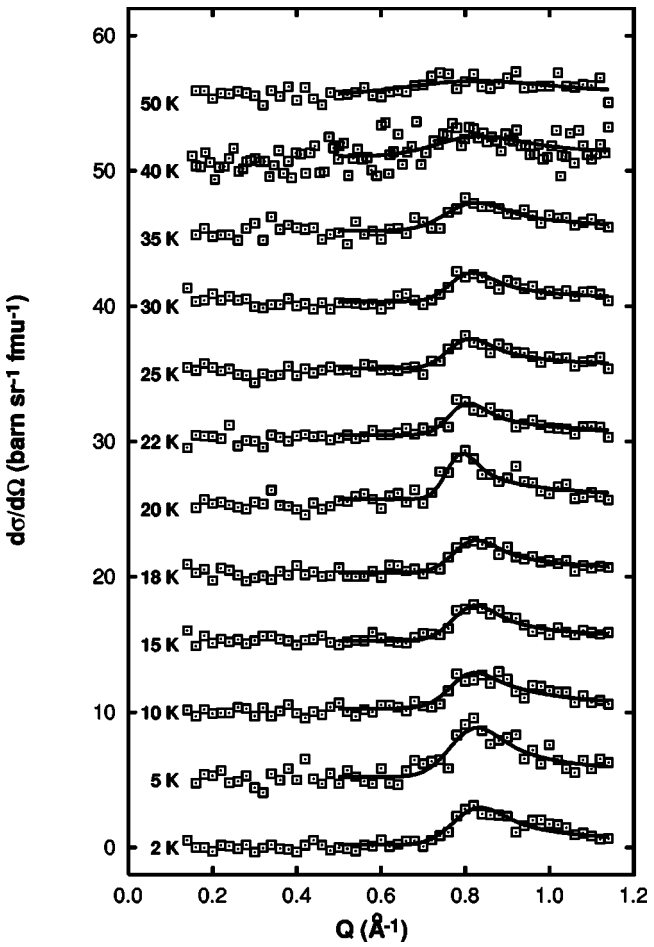

FIG. 2. The differential magnetic scattering cross-section $d\sigma/d\Omega$ of $(d_{20}\text{-PPh}_4)[\text{Fe}_2(\text{ox})_3]$. The solid lines correspond to a fit to a Warren function as is discussed in the text.

Laue-Langevin (ILL), Grenoble, France. The incident beam of cold neutrons, wavelength 4.84 Å, is polarized by a supermirror. Thirty-two ^{3}He detectors, arranged in four banks, each have their own supermirror analyzer. A set of three Helmholz coils allows the polarization direction of the incident beam to be defined along *x*, *y*, or *z*. The disk chopper which permits time-of-flight energy analysis was not present for these measurements.

Two polycrystalline samples of $(d_{20}\text{-PPh}_4)[\text{Fe}^{\text{II}}\text{Fe}^{\text{III}}(\text{ox})_3]$ of mass 3.58 and 7.30 g were mounted in an ILL Orange cryostat in a cylindrical vanadium can. Measurements were performed at 2, 5, 10, 15, 18, 20, 22, 25, 30, 35, 40, and 50 K. At each temperature, full *xyz* polarization analysis[22] was carried out, the spin-flip and non-spin-flip scattering being measured with the incident beam polarization direction along each of the three axes. This enables the total scattering to be separated into its nuclear coherent, spin incoherent, and magnetic components. Data were collected over the range $0.15 \leqslant Q \leqslant 2.5$ Å^{-1}, and parts of these data, the fits of which are discussed below, are shown in Fig. 2. The data are to scale but each successive profile is vertically displaced by 5 b sr^{-1} per formula unit at each temperature. All measurements were corrected for the scattering of the vanadium can and normalized to the scattering of a known mass of vanadium powder or foil, giving an absolute measure of the scattering intensity as a function of *Q*.

D. Mössbauer spectra

The Mössbauer spectral absorbers contained 75 mg/cm^2 of powder and the spectra were measured between 1.9 and 293 or 315 K on a constant-acceleration spectrometer which utilized a room-temperature rhodium matrix cobalt-57 source and was calibrated at room temperature with α-iron foil. The estimated absolute errors are ± 0.01 mm/s for the isomer shifts, ± 0.02 mm/s for the quadrupole splittings and linewidths, and $\pm 2\%$ for the percentage areas of the spectral components. The relative errors are estimated to be smaller by a factor of about one-half.

III. RESULTS AND DISCUSSION

A. Magnetization

The magnetization of $(\text{NBu}_4)[\text{Fe}^{\text{II}}\text{Fe}^{\text{III}}(\text{ox})_3]$ has been reported earlier,[4,6,20,23] and its magnetization and that of $(d_{20}\text{-PPh}_4)[\text{Fe}^{\text{II}}\text{Fe}^{\text{III}}(\text{ox})_3]$ used herein have been measured and are shown in Fig. 1. As expected the magnetization of $(d_{20}\text{-PPh}_4)[\text{Fe}^{\text{II}}\text{Fe}^{\text{III}}(\text{ox})_3]$ corresponds to that of a Néel class-*Q* ferrimagnet[7] and shows a constant, essentially zero value above 30 K and a monotonically increasing value reaching ca. 210 erg Oe^{-1} mol^{-1} under 100 Oe below 30 K, a small value as expected for the ferrimagnetic coupling between high-spin iron(II) and high-spin iron(III). In contrast the magnetic properties of $(\text{NBu}_4)[\text{Fe}^{\text{II}}\text{Fe}^{\text{III}}(\text{ox})_3]$ are quite different, as discussed earlier,[4,6,20,23] and correspond to a Néel class-*N* ferrimagnet.[7]

B. Polarized neutron diffraction

Figure 2 shows the differential magnetic cross section $d\sigma/d\Omega$ of $(d_{20}\text{-PPh}_4)[\text{Fe}^{\text{II}}\text{Fe}^{\text{III}}(\text{ox})_3]$ at temperatures between 2 K and 50 K. Because no structure is observed in the magnetic scattering for $0.15 \leqslant Q \leqslant 0.5$ Å^{-1}, the observed intensity must be due to paramagnetic scattering. The numerical integration of the magnetic intensity over the *Q* range $0.15 \leqslant Q \leqslant 0.50$ Å^{-1} gives an estimate of the relative proportion of fluctuating, uncorrelated spins present. The percentage of the paramagnetic scattering that is expected to fall in this *Q* range can be calculated from the magnetic form factors for Fe^{II} and Fe^{III} as 12.72%.[24] Normalizing to this percentage and the total magnetic scattering over the whole *Q* range gives the percentage of uncorrelated magnetic moments, shown in Fig. 3.

While the uncertainties in this measurement are high, it is still clear that three different scattering regimes can be distinguished. At low temperatures $T \leqslant 10$ K, the paramagnetic intensity is very low. In the intermediate regime $10 < T \leqslant 30$ K, it becomes somewhat higher, while for $T > 30$ K it is higher still. This result is in clear agreement with the analysis of the Mössbauer spectra presented in the following section.

As can be seen in Fig. 2 even at 2 K, the lowest temperature studied, no magnetic Bragg scattering was found over the entire *Q* range studied. This indicates the absence of any

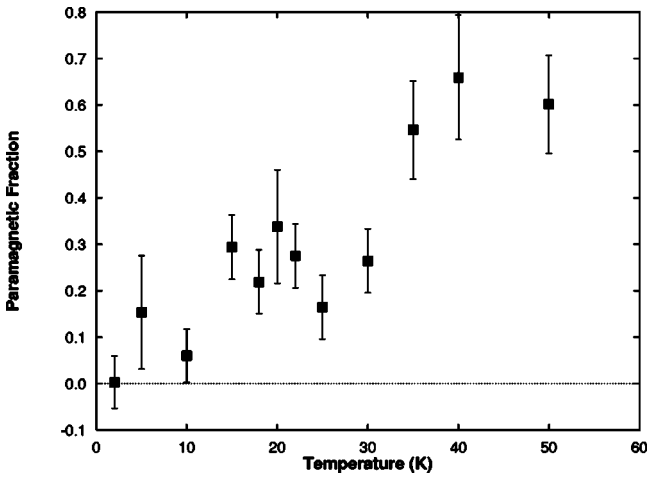

FIG. 3. The paramagnetic intensity integrated over the Q range of $0.15 \leqslant Q \leqslant 0.50$ Å^{-1}, normalized to give the fraction of paramagnetic scattering, as a function of temperature for $(d_{20}\text{-PPh}_4)[\text{Fe}_2(\text{ox})_3]$.

three-dimensional long-range magnetic order in $(d_{20}\text{-PPh}_4)[\text{Fe}^{\text{II}}\text{Fe}^{\text{III}}(\text{ox})_3]$. However, a broad and asymmetric feature is apparent at $Q_0 \approx 0.8$ Å^{-1}, a feature which becomes weaker and broader above 35 K but is still present at 50 K. This non-Bragg scattering is ascribed to quasi-two-dimensional (2D) short-range magnetic correlations and can be described by a Warren function[25,26]

$$p(\theta) = KmF_{hk}^2 \frac{(1+\cos^2 2\theta)}{2(\sin\theta)^{3/2}} \left(\frac{\xi}{\lambda\sqrt{\pi}}\right)^{1/2} F(a), \qquad (1)$$

where λ is the neutron wavelength, K is a scale factor, m is the multiplicity of the 2D reflection $[hk]$ whose structure factor is F_{hk} and whose position is θ_0, ξ is the spin-spin correlation length, and

$$F(a) = \int_0^\infty \exp[-(x^2-a)^2]dx, \qquad (2)$$

where

$$a = \frac{2\xi\sqrt{\pi}}{\lambda}(\sin\theta - \sin\theta_0). \qquad (3)$$

Based on the unit cell parameters determined from the previous, unpolarized neutron diffraction measurements,[9] the scattering intensity at 0.8 Å^{-1} was assigned as [20]. Because the integral in Eq. (2) cannot be solved analytically, the function was integrated numerically to an upper limit of 20 with results that compare favorably with those given in Ref. 26. Fitting the Warren-like feature therefore yields the temperature dependence of the 2D correlation length. Fits were performed for each temperature in the Q range $0.5 \leqslant Q \leqslant 1.15$ Å^{-1} and are shown at each temperature in Fig. 2.

The variation of the magnetic exchange correlation length with temperature in $(d_{20}-\text{PPh}_4)[\text{Fe}^{\text{II}}\text{Fe}^{\text{III}}(\text{ox})_3]$ is shown in Fig. 4.

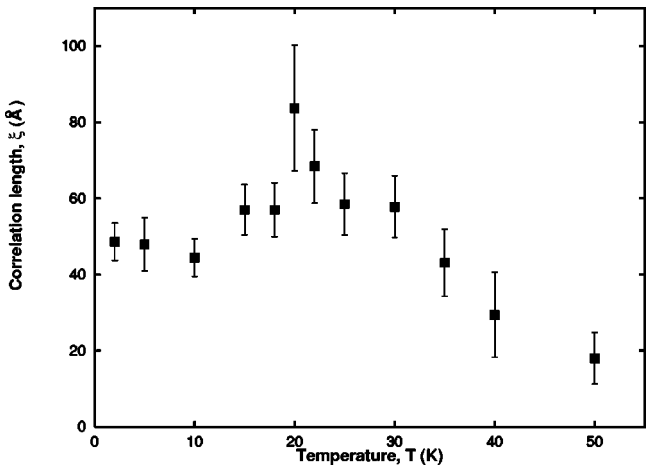

FIG. 4. The two-dimensional magnetic correlation length ξ as a function of temperature for $(d_{20}\text{-PPh}_4)[\text{Fe}_2(\text{ox})_3]$.

As expected, above 30 K the correlation length decreases with increasing temperature in the paramagnetic phase. Below 30 K, rather unexpectedly, the correlation length increases only slightly and reaches a maximum of only ca. 80 Å at 20 K. These results seem to indicate a small decrease in the correlation length, a decrease that may be an artifact of the two samples used for this study; most likely the correlation length is unchanging at ca. 50 Å below 20 K. This distance corresponds to between five and six honeycomb units.

The diffraction observed here, while not conclusive, is compatible with an orientation of the magnetic moments in the basal plane. On the basis of their unpolarized neutron diffraction work on $(d_{20}-\text{PPh}_4)\text{Mn}^{\text{II}}\text{Fe}^{\text{III}}(\text{ox})_3$, which does exhibit long-range magnetic order, Nuttall and Day[9] concluded that the moments in this compound are axial, an orientation that seems reasonable for a magnetic compound with an $^6A_{1g}$ ground state for both ions and, hence, no orbital contribution to the magnetic anisotropy. In contrast, in $(d_{20}-\text{PPh}_4)[\text{Fe}^{\text{II}}\text{Fe}^{\text{III}}(\text{ox})_3]$ the iron(II) ion does have a significant orbital contribution to the magnetic moment, as discussed below, and hence its contribution to the magnetic anisotropy may be quite different. As a consequence the magnetic moments in $(d_{20}-\text{PPh}_4)[\text{Fe}^{\text{II}}\text{Fe}^{\text{III}}(\text{ox})_3]$ may be basal, an orientation which would lead to a threefold degeneracy, giving rise to three energetically equivalent easy directions of magnetization. In this case the spin configurational entropy may limit the exchange correlation length and the direction of the exchange-correlated moments may be different, depending on their nucleation site.

C. Mössbauer spectral analysis

1. Paramagnetic spectra

The Mössbauer spectra of $(\text{PPh}_4)[\text{Fe}_2(\text{ox})_3]$ and $(\text{NBu}_4)[\text{Fe}_2(\text{ox})_3]$ have been measured as a function of temperature and selected paramagnetic spectra are shown in Figs. 5 and 6, respectively.

The experimental data shown in these figures clearly indicate the presence of two quadrupole doublets, which may

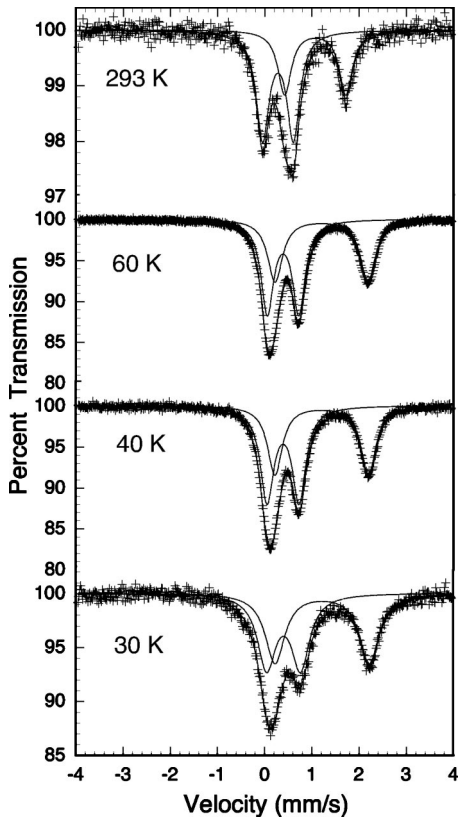

FIG. 5. Selected paramagnetic Mössbauer spectra of $(PPh_4)[Fe_2(ox)_3]$ obtained at the indicated temperatures.

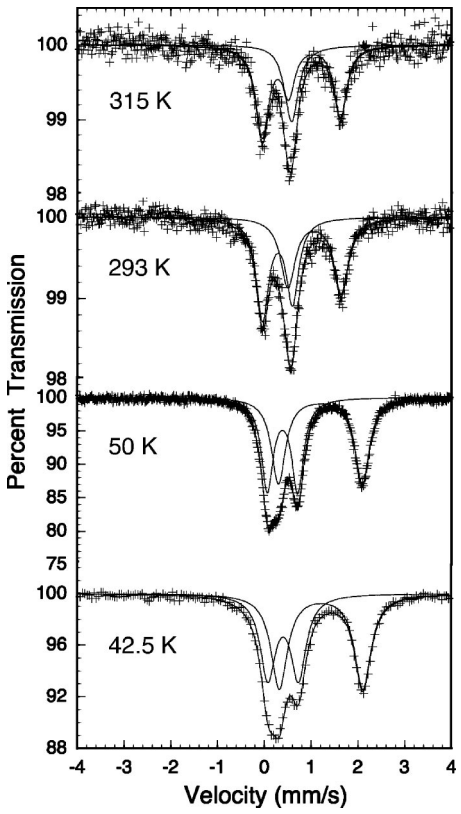

FIG. 6. Selected paramagnetic Mössbauer spectra of $(NBu_4)[Fe_2(ox)_3]$ obtained at the indicated temperatures.

be assigned to iron(II) and iron(III) ions. Although the fits shown in these figures are not unique in terms of the placement of the two lines found at ca. 0.0 mm/s, they do yield hyperfine parameters which are consistent both with earlier studies, summarized in Table I, and with the parameters obtained for the magnetically ordered spectra, which are discussed in detail in the next section. Further, these fits yield hyperfine parameters which are physically realistic for high-spin iron(II) and iron(III) ions in the distorted octahedral coordination environment expected in these compounds. The resulting hyperfine parameters are given in Tables II and III for $(PPh_4)[Fe_2(ox)_3]$ and $(NBu_4)[Fe_2(ox)_3]$, respectively.

The Mössbauer spectra of $(PPh_4)[Fe_2(ox)_3]$ shown in Fig. 5 clearly indicate that this compound is paramagnetic between 293 and 40 K. Although the spectrum observed at 30 K is similar to the 40 K spectrum, the lines are clearly broader, an indication of the onset of magnetic exchange correlations. As will be seen in the next section, the spectra of $(PPh_4)[Fe_2(ox)_3]$ clearly show the influence of magnetic exchange correlations at 25 K and below. In contrast, the spectra of $(NBu_4)[Fe_2(ox)_3]$ shown in Fig. 6 indicate that it is paramagnetic between 315 and 50 K. Although the spectrum observed at 42.5 K is similar to the 50 K spectrum, the lines are broader, again an indication of the onset of magnetic exchange correlations. As will be seen in the next section, the spectra of $(NBu_4)[Fe_2(ox)_3]$ clearly show the influence of magnetic exchange correlations at 40 K and below.

The isomer shifts of the iron(II) sites in the two compounds are very similar at 1.12 and 1.16 mm/s at 293 K, values which are characteristic of high-spin iron(II). The isomer shifts of the iron(III) sites in the two compounds are virtually identical at 0.39 and 0.38 mm/s at 293 K, values which are characteristic of high-spin iron(III). The isomer shift values are very similar to those observed[27–29] for iron(II) in $Fe(ox)\cdot 2H_2O$ and iron(III) in $K_3Fe(ox)_3$ and confirm the assignments presented in Tables II and III. Further, the paramagnetic spectra are very similar to those reported earlier[3,13,15] and the spectra reported by Coronado *et al.*[19] for $[FeCp_2^*][Fe_2(ox)_3]$ except for the presence of an additional line due to the $(FeCp_2^*)$ cation. The observed decrease in the isomer shifts of $(PPh_4)[Fe_2(ox)_3]$ and $(NBu_4)[Fe_2(ox)_3]$ with increasing temperature (see Tables II and III) results from the second-order Doppler-shift contribution to the isomer shift and validate the analysis.

As is revealed in Tables II and III, the quadrupole splittings of the iron(III) sites are similar and almost independent of temperature in both $(PPh_4)[Fe_2(ox)_3]$ and $(NBu_4)[Fe_2(ox)_3]$ with respective values of -0.64 and -0.65 mm/s at 293 K. The values are negative as is required to obtain the *best* fit of the magnetically ordered spectra, but the equivalent positive values may be equally acceptable; see discussion below. The slightly larger magnitude of the quadrupole splittings observed for $(PPh_4)[Fe_2(ox)_3]$ at lower temperatures may indicate that larger distortions in its iron(III) coordination environment are produced on cooling; the same trend is observed for the iron(II) site in this complex.

TABLE I. Previous Mössbauer spectral studies of $(NBu_4)[M^{II}M^{III}(ox)_3]$.

Site	M^{II}	M^{III}	T (K)	δ (mm/s)[b]	ΔE_Q (mm/s)	V_{zz}[a]	H_{eff} (kOe)	θ (deg)	Ref.
Fe^{II}	Fe	Fe	78	1.30	1.79	±	0		3
			4.2	1.32	1.92	−	52	90	11
	Fe	Cr	298	1.18	1.26	±	0		3
			12	1.33	1.82	±	0		
			10	1.32	1.85	−	35	90	
			4.2	1.33	1.86	−	38	90	
	Fe	Cr	293	1.18	1.23	±	0		15
			4.2		1.78	−	45	90	
Fe^{III}	Fe	Fe	78	0.51	0.60	±	0		3
			4.2		0.60	+	537	81	11
					0.60	−	537	37	
	Mn	Fe	78	0.49	0.62	±	0		11
			30	0.50	0.62	±	0		
			25	0.50	0.62	+	320	52	
			20	0.51	0.62	+	380	58	
			15	0.49			432		
			4.2	0.50			502		
	Ni	Fe	78	0.49	0.68	±	0		11
			25	0.51	0.71	±	0		
			20	0.50	0.71	+	391	28	13
			4.2	0.50	0.71	+	509	28	

[a]± indicates that either the sign was unknown or not reported.
[b]The isomer shifts are given relative to room-temperature α-iron foil.

In contrast to the iron(III) sites and, as expected[30] for a high-spin iron(II) ion with the approximate $t_{2g}^4 e_g^2$ electronic configuration in a distorted octahedral coordination environment, the quadrupole splittings for the iron(II) sites in both $(PPh_4)[Fe_2(ox)_3]$ and $(NBu_4)[Fe_2(ox)_3]$ are rather different and decrease dramatically with increasing temperature above ca. 50 K, the change being larger for $(PPh_4)[Fe_2(ox)_3]$ than for $(NBu_4)[Fe_2(ox)_3]$. The temperature dependence for both compounds is shown in Fig. 7, where again the quadrupole splitting values are taken to be negative as is required to best fit the ordered spectra.

The temperature dependence of the iron(II) quadrupole splitting ΔE_Q in a distorted environment may be fitted with the Ingalls model[30] in which

$$\Delta E_Q = \Delta E_Q(0)\tanh\left(\frac{\Delta}{2kT}\right), \tag{4}$$

where $\Delta E_Q(0)$ is the quadrupole splitting at 0 K and Δ is the splitting of the orbital triplet $^5T_{2g}$ octahedral iron(II) ground state by low-symmetry components of the crystal field. The solid lines shown in Fig. 7 correspond to the best fits of the quadrupole splittings with this model. For $(PPh_4)[Fe_2(ox)_3]$ the best-fit parameters are $\Delta E_Q(0) = 1.98$ mm/s, $V_{zz} = -9.06\times10^{21}$ V/m^2, and $\Delta = 292$ cm^{-1} and for $(NBu_4)[Fe_2(ox)_3]$ they are $\Delta E_Q(0) = 1.79$ mm/s, $V_{zz} = -8.19\times10^{21}$ V/m^2, and $\Delta = 312$ cm^{-1}. The fits with this model are not fully adequate, most probably because of small changes in Δ with temperature, which are ignored by the Ingalls model. Changes in Δ with temperature are not unexpected in complexes of the type studied here, as a result of anisotropic changes in the coordination environment of the iron(II) sites.

TABLE II. Mössbauer spectral hyperfine parameters for $(PPh_4)[Fe_2(ox)_3]$.

Site	T (K)	δ (mm/s)[a]	ΔE_Q (mm/s)	V_{zz} (10^{21} V/m^2)	H_{max} (kOe)	Γ (mm/s)	Area (%)
Fe^{II}	293	1.123	1.30	−5.95		0.34	39
	240	1.169	1.42	−6.50		0.25	40
	190	1.217	1.55	−7.09		0.29	42
	140	1.248	1.70	−7.78		0.30	41
	90	1.275	1.88	−8.60		0.33	43
	60	1.299	1.97	−9.02		0.38	45
	40	1.307	1.98	−9.06		0.35	45
	30	1.317	2.00	−9.15		1.12	51
	25	1.307	1.98[b]	−9.06	40	1.40	52
	22.5	1.307	1.98[b]	−9.06	55	1.23	54
	20	1.304	1.98[b]	−9.06	61	0.95	51
	15	1.337	1.98[b]	−9.06	68	0.85	46
	10	1.306	1.98[b]	−9.06	68	0.84	43
	6	1.338	1.98[b]	−9.06	65	0.91	45
	4.2	1.316	1.98[b]	−9.06	65	0.83	44
	1.9	1.329	1.98[b]	−9.06	68	0.78	43
Fe^{II}	293	0.390	0.65	−2.98		0.33	61
	240	0.410	0.60	−2.75		0.35	60
	190	0.440	0.60	−2.75		0.35	58
	140	0.467	0.62	−2.84		0.32	59
	90	0.479	0.63	−2.88		0.33	57
	60	0.486	0.67	−3.07		0.32	55
	40	0.488	0.68	−3.11		0.35	55
	30	0.500	0.72	−3.30		0.47	49
	25	0.493	0.72	−3.30	460	0.98	48
	22.5	0.479	0.72	−3.30	485	1.02	46
	20	0.494	0.75	−3.43	500	1.24	49
	15	0.507	0.75	−3.43	520	0.64	54
	10	0.512	0.75	−3.43	526	0.52	57
	6	0.517	0.78	−3.57	527	0.56	55
	4.2	0.532	0.74	−3.39	540	0.38	56
	1.9	0.527	0.72	−3.30	541	0.42	57

[a]The isomer shifts are given relative to room-temperature α-iron foil.
[b]Parameter constrained to the value given.

2. Magnetically ordered spectra

The magnetically ordered Mössbauer spectra of $(PPh_4)[Fe_2(ox)_3]$ and $(NBu_4)[Fe_2(ox)_3]$ are shown in Figs. 8 and 9, respectively. It should be noted that the spectra shown in Figs. 8 and 9 are again qualitatively very similar to those reported earlier[3,13,15,16,18] and by Coronado *et al.*[19] for $[FeCp_2^*][Fe_2(ox)_3]$ except for the presence of an additional line due to the $(FeCp_2^*)$ cation.

TABLE III. Mössbauer spectral hyperfine parameters for $(NBu_4)[Fe_2(ox)_3]$.

Site	T (K)	δ (mm/s)[a]	ΔE_Q (mm/s)	V_{zz} (10^{21} V/m^2)	H_{max} (kOe)	Γ (mm/s)	Area (%)
Fe^{II}	315	1.162	1.12	−5.13		0.33	44
	293	1.164	1.14	−5.22		0.38	48
	240	1.204	1.34	−6.13		0.32	46
	190	1.235	1.42	−6.50		0.31	47
	140	1.265	1.60	−7.32		0.31	47
	90	1.291	1.72	−7.87		0.30	49
	50	1.290	1.79	−8.19		0.36	53
	45	1.306	1.78	−8.15		0.39	52
	42.5	1.306	1.79	−8.19		0.43	55
	40	1.306	1.79[b]	−8.19	38	0.82	58
	39	1.315	1.79[b]	−8.19	38	0.98	65
	38	1.312	1.79[b]	−8.19	45	0.81	60
	35	1.275	1.79[b]	−8.19	40	0.75	52
	30	1.319	1.79[b]	−8.19	50	1.10	50
	10	1.331	1.79[b]	−8.19	58	0.68	47
	4.2	1.327	1.79[b]	−8.19	57	0.59	47
	1.9	1.329	1.79[b]	−8.19	58	0.59	48
Fe^{III}	315	0.363	0.63	−2.88		0.33	56
	293	0.380	0.64	−2.93		0.32	52
	240	0.416	0.65	−2.98		0.40	54
	190	0.435	0.65	−2.98		0.35	53
	140	0.461	0.64	−2.93		0.32	53
	90	0.486	0.64	−2.93		0.29	51
	50	0.481	0.65	−2.98		0.36	47
	45	0.489	0.65	−2.98		0.37	48
	42.5	0.495	0.66	−3.02		0.39	45
	40	0.504	0.67	−3.07	360	0.78	42
	39	0.518	0.64	−2.93	405	0.92	35
	38	0.518	0.64	−2.93	405	1.08	40
	35	0.518	0.64	−2.93	428	1.02	48
	30	0.518	0.67	−3.07	462	0.72	50
	10	0.503	0.68	−3.11	530	0.44	53
	4.2	0.520	0.67	−3.07	544	0.31	53
	1.9	0.520	0.66	−3.02	545	0.29	52

[a]The isomer shifts are given relative to room-temperature α-iron foil.

[b]Parameter constrained to the given value.

The spectra shown in Figs. 8 and 9 have been fitted with a minimization program[31] which calculates the eigenvalues and eigenvectors of the ground- and excited-state Hamiltonians describing the combined quadrupolar and magnetic interactions. The adjustable hyperfine parameters for a given component in the spectral fits are the isomer shift δ, the effective hyperfine field $H_{\rm eff}$, the quadrupole interaction ΔE_Q, the angle θ between the principle axis of the electric field gradient and the magnetization direction, and the linewidth Γ. In all fits reported herein $\eta = 0.0$ as is expected for the axially symmetric trigonal iron(II) and iron(III) sites in these complexes. Further, any attempt to increase the value of the asymmetry parameter η above zero leads to substantially poorer fits. Thus the spectra were fit by adjusting the five adjustable parameters for each spectral component and by using enough spectral components to reproduce the experimental spectrum. In addition, at a given temperature, the δ, ΔE_Q, and Γ values associated with a given iron oxidation state have been constrained to be equal. In contrast, in none of the fits have the relative areas of the iron(II) and iron(III) components been constrained.

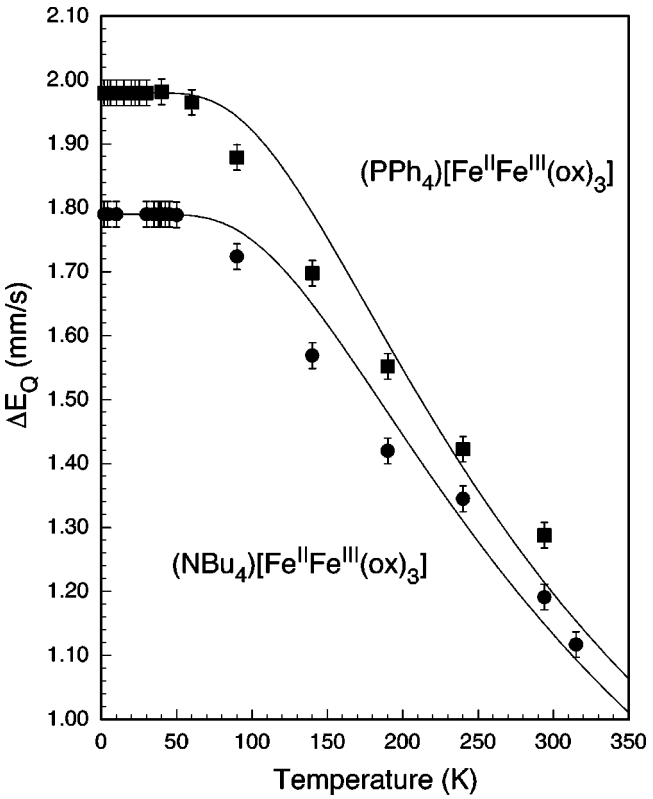

FIG. 7. The temperature dependence of the iron(II) quadrupole interactions of $(PPh_4)[Fe_2(ox)_3]$ (■) and $(NBu_4)[Fe_2(ox)_3]$ (●). The absolute error bars are shown. The solid lines represent a fit of the quadrupole splittings based on the Ingalls model as is discussed in the text.

In the spectra shown in Figs. 8 and 9 it is immediately apparent that the iron(III) ions exhibit a sextet with a large hyperfine field. In contrast, the iron(II) ions exhibit a relatively small hyperfine field. The presence of these sextets would seem to indicate the presence of long-range magnetic order in these complexes, a presence which initially appears inconsistent with the polarized neutron diffraction results presented above for $(PPh_4)[Fe_2(ox)_3]$.

Below 10 K for $(PPh_4)[Fe_2(ox)_3]$ and below 30 K for $(NBu_4)[Fe_2(ox)_3]$ the Mössbauer spectra show sharp sextets, which indicate that the short-range magnetic exchange correlations observed in the polarized neutron scattering study yield an apparently static hyperfine field at both iron sites. Between 10 and 30 K for $(PPh_4)[Fe_2(ox)_3]$ and between 30 and 45 K for $(NBu_4)[Fe_2(ox)_3]$, the Mössbauer spectra are a superposition of broadened sextets and paramagnetic doublets. We believe that this behavior results from the dynamic behavior of the short-range magnetic exchange correlations. Each layer within a compound can be envisaged

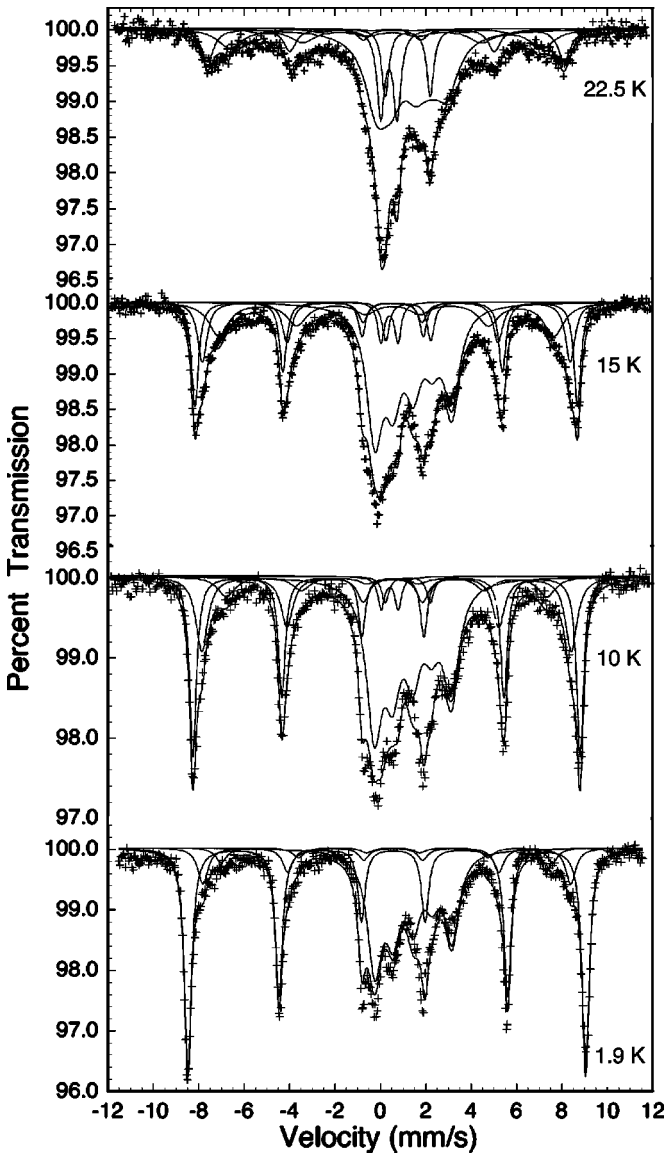

FIG. 8. Selected Mössbauer spectra of $(PPh_4)[Fe_2(ox)_3]$ obtained at the indicated temperatures.

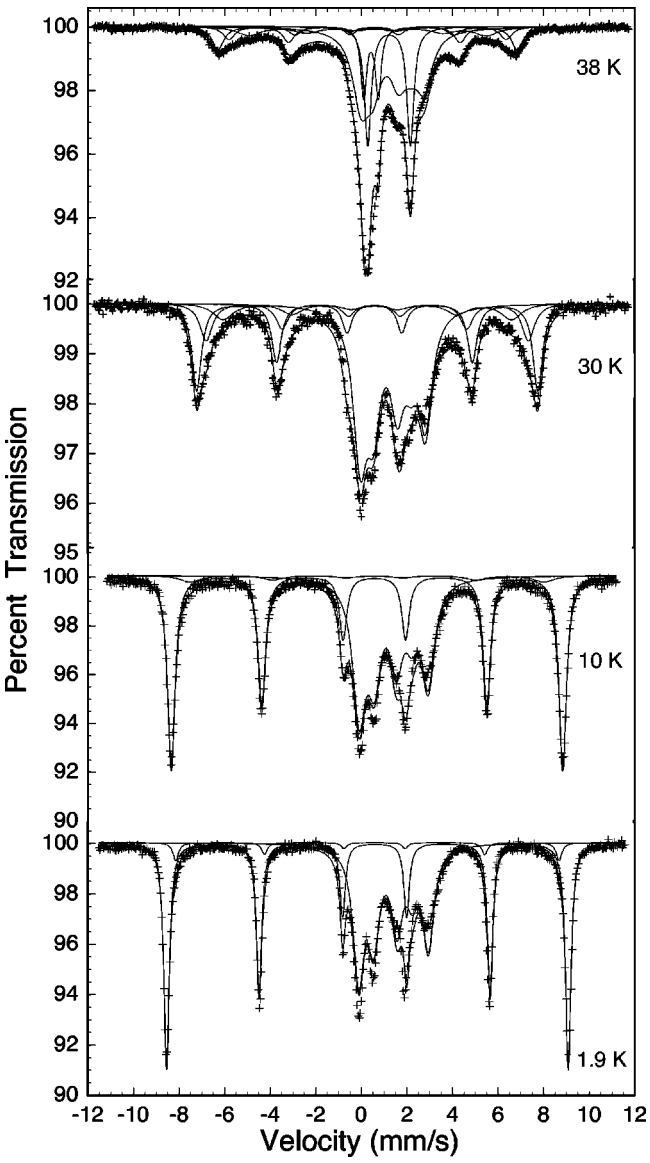

FIG. 9. Selected Mössbauer spectra of $(NBu_4)[Fe_2(ox)_3]$ obtained at the indicated temperatures.

as composed of small regions of ca. 50 Å diameter, in which there is magnetic exchange correlation. The Mössbauer spectrum will depend on the lifetime of this correlation. At the lowest temperatures, the lifetime is longer than the Larmor period of the nuclear moment and the Mössbauer spectra show sharp sextets. As the temperature increases, the lifetime decreases and a given iron nucleus then sees a relaxing hyperfine field which gives rise to the broadened sextets or the paramagnetic doublets, depending upon the relaxation rate. Hence the Mössbauer spectra probe the time domain of the short-range magnetic exchange correlations observed by polarized neutron scattering. More specifically, at 1.9 K the relaxation time of the hyperfine field is longer than the Larmor precession period of the nuclear moment, a period which can be obtained from the splitting of the outer lines of the Fe(III) sextet. In other words, the relaxation time is at least one order of magnitude longer than the Larmor period of 0.5×10^{-8} s. As the temperature increases, the relaxation time becomes smaller and paramagnetic doublets are observed if the relaxation time is at least one order of magnitude shorter than the Larmor period of 0.5×10^{-8} s. The broadened sextets correspond to intermediate relaxation times between 10^{-7} and 10^{-9} s. Because a superposition of sextets and doublets is observed, there is a distribution of relaxation times within the layer. As expected, the relative area of the paramagnetic doublets increases as the temperature approaches the critical temperature.

The preliminary fits also indicated that more than one magnetic sextet was required to fit the spectral components associated with the iron(III) ions, even at the lowest temperatures of 4.2 and 1.9 K. At higher temperatures these magnetic sextets are quite broad, presumably because of differing relaxation rates of the hyperfine fields due to the dynamic nature of the short-range magnetic exchange correlations within the layers. In contrast to the iron(III) site, only one magnetic component was required to fit the iron(II) contri-

bution to the spectra but in this case, the very much reduced hyperfine field would be less sensitive to variations in the magnetic environment. Further, the failure of our model to more adequately fit the observed spectral profile of the iron(II) sextet is an indication of the presence of some variation in the magnetic environment.

As expected from the quadrupole splitting observed in the paramagnetic spectra, the magnetic spectra of $(PPh_4)[Fe_2(ox)_3]$ and $(NBu_4)[Fe_2(ox)_3]$ exhibit quadrupole shifts (QS's). These quadrupole shifts are most easily observed in the spectra as a difference in the splitting of 1 and 2 and 5 and 6 iron(III) lines at 1.9 K. Because the quadrupole shift is determined by *both* the quadrupole splitting ΔE_Q and θ through the equation

$$\mathrm{QS}=\frac{1}{2}\Delta E_Q(3\cos^2\theta-1), \tag{5}$$

it is not possible to determine both ΔE_Q and θ from the magnetic spectra. Fortunately, it is well known[31] that ΔE_Q approaches a constant value at low temperatures. Hence, in fitting the iron(II) component of the magnetic spectra, ΔE_Q was constrained to be equal to the value observed in the lowest-temperature paramagnetic spectrum and the θ value was adjusted to yield the observed quadrupole shift. Essentially the same approach was used for the iron(III) components except that it was found unnecessary to fix the ΔE_Q and θ values, which could easily be estimated from the observed spectra. For the iron(II) sextet the *best* fits always corresponded to $V_{zz}<0$ and θ values of 90°; no acceptable fits could be obtained with positive V_{zz}. Further, for the iron(III) sextets the *best* fits always corresponded to a negative V_{zz} and θ values of ca. 40°; the results of these *best* fits are shown in Figs. 10 and 11. However, for the iron(III) sextets it was found that alternative fits with a positive V_{zz} and θ values which are much closer to 90° were almost as good as the best fits. At 1.9 K the alternative fit for $(PPh_4)[Fe_2(ox)_3]$ corresponds to $\Delta E_Q=0.75$ mm/s, $V_{zz}>0$, and $\theta=72.4°$ and the alternative fit for $(NBu_4)[Fe_2(ox)_3]$ corresponds to $\Delta E_Q=0.67$ mm/s, $V_{zz}>0$, and $\theta=81.1°$. A comparison of these alternative fits with the fits shown in Figs. 10 and 11 indicates that the alternative fit is potentially acceptable.

If the principal axis of the electric field gradient tensor at the iron site is reasonably assumed to be the *c* axis, the θ angle of 90° for the iron(II) site indicates that the iron(II) hyperfine field is within the plane of the layer. A similar conclusion was reached by Iijima and Mizutani[11] for $(NBu_4)[Fe_2(ox)_3]$. If the effective hyperfine field is assumed to be parallel to the iron moment, then the iron(II) Mössbauer spectral fit and hyperfine parameters are fully consistent with a basal orientation of the moments.

In the case of the iron(III) sextet, if the negative quadrupole interaction values are used, the θ angles are $40°\pm1°$ and ca. $37°\pm1°$ for $(PPh_4)[Fe_2(ox)_3]$ and $(NBu_4)[Fe_2(ox)_3]$, respectively, and indicate that the iron(III) hyperfine fields and moments are canted from the *c* axis. If the positive quadrupole interaction values are used, the θ angles are $72°\pm1°$ and ca. $81°\pm1°$ for

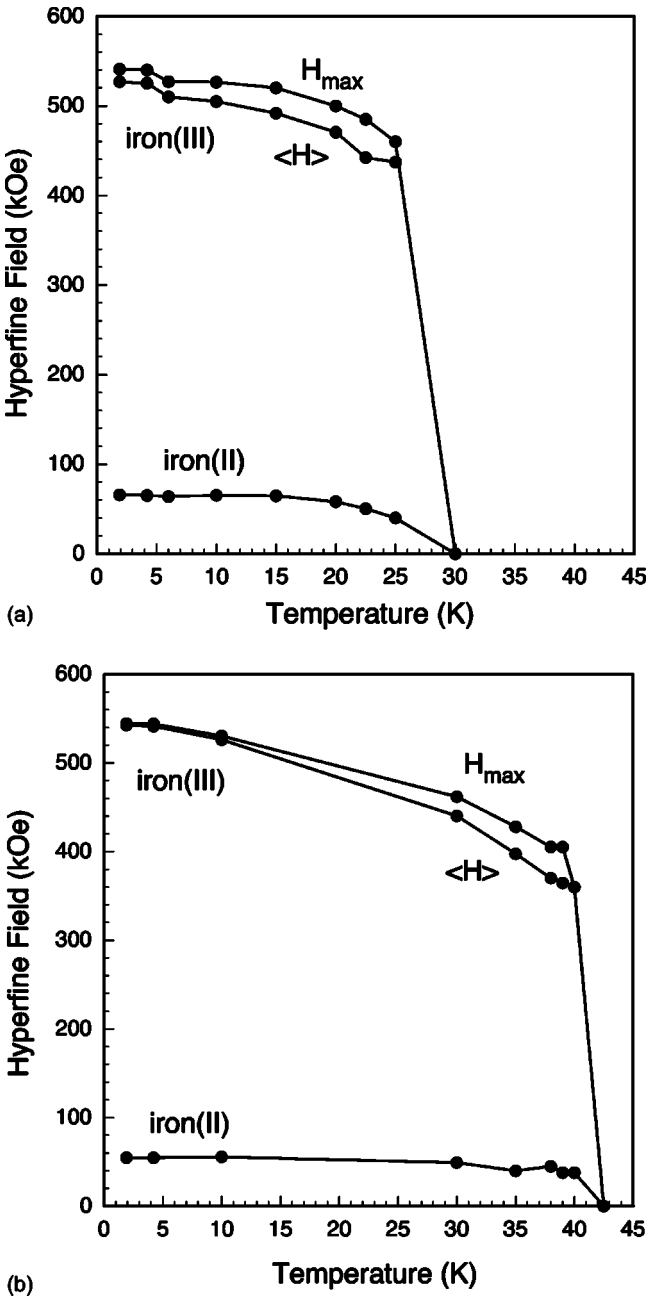

FIG. 10. The temperature dependence of the maximum hyperfine field H_{max} and the weighted average hyperfine field $\langle H\rangle$ for iron(III) and the hyperfine field for iron(II) in $(PPh_4)[Fe_2(ox)_3]$ (a) and in $(NBu_4)[Fe_2(ox)_3]$ (b).

$(PPh_4)[Fe_2(ox)_3]$ and $(NBu_4)[Fe_2(ox)_3]$, respectively, and indicate that the iron(III) hyperfine field and moments are close to the basal plane. In either case, there is a component of the moments in the basal plane. So the magnetically ordered Mössbauer spectra are certainly consistent with a basal orientation of the iron magnetic moments in both $(PPh_4)[Fe_2(ox)_3]$ and $(NBu_4)[Fe_2(ox)_3]$. They suggest that perhaps there is either some canting of the moments or some noncollinearity of the iron(II) and iron(III) moments.

In attempting to fit the spectra obtained just below the apparent freezing temperature, it was found that no accept-

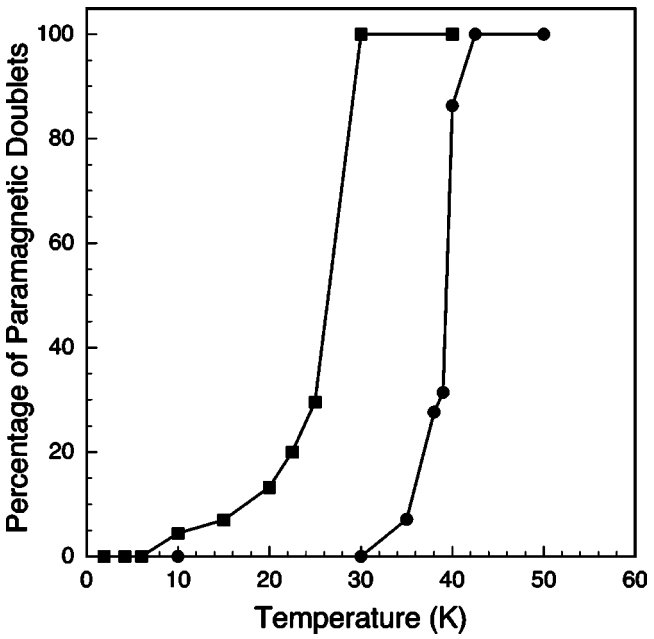

FIG. 11. A comparison of the percentage area of the paramagnetic quadrupole doublets observed in the Mössbauer spectra of $(PPh_4)[Fe_2(ox)_3]$ (■) and $(NBu_4)[Fe_2(ox)_3]$ (●) as a function of temperature.

able fits could be obtained unless the fit also included paramagnetic components, which were constrained to have the same δ, ΔE_Q, and Γ values as the magnetic components of the spectra. The necessity of including these paramagnetic components is most easily observed in the 22.5 K spectrum of $(PPh_4)[Fe_2(ox)_3]$ shown in Fig. 8 and the 38 K spectrum of $(NBu_4)[Fe_2(ox)_3]$ shown in Fig. 9. The presence of these paramagnetic components is consistent with the magnetic properties discussed above. At the temperatures requiring these components, a portion of the iron ions experience a rapidly fluctuating hyperfine field because of the dynamic nature of the exchange correlated regions within the layers.

The fits of the magnetic spectra yield isomer shifts and quadrupole splittings that are reasonable and consistent with the values obtained from the paramagnetic spectra: see Tables II and III and Fig. 7. Further, in all cases, the unconstrained ratio of iron(II) to iron(III) spectral areas is close to 50:50 in agreement with the small iron(II) deficiency observed experimentally in these compounds.[23] The 0 K extrapolated values of the iron(II) percentages are 48% and 45% in $(NBu_4)Fe_2(ox)_3$ and $(PPh_4)Fe_2(ox)_3$, respectively.

The magnetic hyperfine fields are shown as a function of temperature in Fig. 10, which shows for the iron(III) spectral components both the maximum field H_{max} and the weighted average field $\langle H \rangle$. For both $(PPh_4)[Fe_2(ox)_3]$ and $(NBu_4)[Fe_2(ox)_3]$ the iron(III) hyperfine fields approach 540 kOe at low temperatures and are typical of high-spin iron(III) with an $S=\frac{5}{2}$ electronic ground state. In contrast, the iron(II) ions in the two compounds have saturation hyperfine fields of ca. 65 and 55 kOe, fields which are much lower than the values of ca. 440 kOe expected of high-spin iron(II) with an $S=2$ electronic ground state. Similar very small iron(II) fields have been reported[3,12] earlier for $(NBu_4)[Fe_2(ox)_3]$.

The effective magnetic hyperfine field, H_{eff}, at the iron site is given[32] by

$$H_{eff}=H_{core}+H_{orb}+H_{dip}, \tag{6}$$

where H_{core} is the Fermi contact term and is typically -440 kOe, and H_{dip} and H_{orb} are the fields produced by the dipolar interaction of the nuclear magnetic moment with the electronic and orbital spin moment, respectively. Usually these last two terms are small. However, in $(PPh_4)[Fe_2(ox)_3]$ and $(NBu_4)[Fe_2(ox)_3]$, the iron(II) orbital moment is not quenched by the trigonal symmetry at the iron(II) site[16,18] and, further, its contribution is expected[33] to oppose that of H_{core}. Thus, from the observed effective hyperfine fields H_{eff}, which are known[15] to be positive, we calculate that $H_{orb}+H_{dip}$ is ca. $+500$ kOe.

A comparison of Figs. 10(a) and 10(b) indicates that the 30 K ordering temperature of $(PPh_4)[Fe_2(ox)_3]$ is substantially lower than the 45 K value observed for $(NBu_4)[Fe_2(ox)_3]$. The latter value is very similar to the 43 K ordering temperature observed[19] for $[FeCp_2^*][Fe_2(ox)_3]$.

Figures 10(a) and 10(b) show that both sublattices order at the same temperature. Further, both hyperfine fields increase at the same rate, contrary to the prediction of Nuttall and Day. For instance, at 30 K just below the compensation temperature of $(NBu_4)[Fe_2(ox)_3]$, both fields have reached 85% of their saturation value. Hence, we do not find any evidence in the temperature dependence of the hyperfine fields to explain the negative magnetization of $(NBu_4)[Fe_2(ox)_3]$. However it is difficult to relate directly the hyperfine fields to the sublattice magnetization, especially for the iron(II) ions because of the large orbital contribution to this field.

It should be noted that the three regions of differing paramagnetic intensity observed in the polarized neutron diffraction results shown in Fig. 3 are also reflected in the percentage area of the paramagnetic doublets observed in the Mössbauer spectra of $(PPh_4)[Fe_2(ox)_3]$ and shown in Fig. 11. Below 10 K, virtually no paramagnetic doublets were observed. Between 10 and 25 K, paramagnetic doublets are required and are consistent with the intermediate intensity of the paramagnetic scattering observed in the polarized neutron diffraction results. Above 30 K, only paramagnetic doublets are observed and the intensity of the paramagnetic scattering is the highest. The analogous results for $(NBu_4)[Fe_2(ox)_3]$ are also shown in Fig. 11 and seem to indicate a parallel behavior to that observed in the $(PPh_4)[Fe_2(ox)_3]$, a parallel behavior which is shifted to higher temperature by ca. 15 K. The similarity would seem to indicate that the magnetic exchange correlations are very similar in the two compounds but the different cations and the presence of additional vacancies in $(PPh_4)[Fe_2(ox)_3]$, as compared to $(NBu_4)[Fe_2(ox)_3]$, lowers the onset of the magnetic exchange correlations by ca. 15 K.

IV. DISCUSSION

The polarized neutron diffraction results reported herein give the first description of the onset of magnetic interactions

in $(d_{20}\text{-}PPh_4)$ $[Fe^{II}Fe^{III}(ox)_3]$. The unexpected result is the absence of long-range magnetic order. In contrast, short-range magnetic correlations are present below ca. 50 K. The existence of small magnetically correlated regions, or domains of ca. 50 Å diameter, within the layer plane is incompatible with iron magnetic moments parallel to the *c* axis. Hence, the iron magnetic moments must lie within the layer plane or at least have a component within the layer plane. This conclusion is in agreement with the analysis of the magnetically ordered Mössbauer spectra. While no neutron diffraction data are available for $(NBu_4)[Fe_2(ox)_3]$, the similarities between the Mössbauer spectra of $(PPh_4)[Fe_2(ox)_3]$ and $(NBu_4)[Fe_2(ox)_3]$ lead to the conclusion that the magnetic behaviors of the two compounds are similar. Particularly, regions of differing paramagnetic intensity are found in both compounds. This suggests that a similar freezing process is involved in the ordering of both compounds. Without polarized neutron diffraction data, however, the spatial extent of the correlated domains in $(NBu_4)[Fe_2(ox)_3]$ cannot be determined.

The magnetic behavior of $(NBu_4)[Fe_2(ox)_3]$ has been interpreted in terms of a spin-glass-like behavior in several previous papers.[11,34–36] This spin-glass-like behavior and the short-range magnetic correlation model proposed herein can be reconciled as follows. As indicated by the chemical analyses both $(PPh_4)[Fe_2(ox)_3]$ and $(NBu_4)[Fe_2(ox)_3]$ are iron deficient, a deficiency which results in a shortage of iron(II) in agreement with the 45% and 48% of iron(II) observed in the Mössbauer spectra of $(PPh_4)[Fe_2(ox)_3]$ and $(NBu_4)[Fe_2(ox)_3]$, respectively. When the temperature decreases below the freezing temperature, small regions or domains of correlated spins form most likely at nucleation sites, sites which may be located near one of the iron(II) vacancies. Because of the three magnetically equivalent directions within the layer plane, these spin-correlated domains grow with a spin direction parallel to one of three equivalent directions. Between these domains, there are regions of uncorrelated spins observed as the paramagnetic scattering in the polarized neutron diffraction profiles and as the paramagnetic doublets in the Mössbauer spectra. As the temperature decreases further, the exchange-correlated spin domains grow at the expense of the uncorrelated regions, as is indicated by the temperature dependence of the paramagnetic contribution to the Mössbauer spectra: see Fig. 11. Below ca. 10 K for $(PPh_4)[Fe_2(ox)_3]$ and 30 K for $(NBu_4)[Fe_2(ox)_3]$ the random spin structure freezes and no paramagnetic doublets are observed in the Mössbauer spectra. In these temperature regions, the spin structure can be viewed as a glass formed by small domains of magnetically correlated spins randomly aligned parallel to one of the three equivalent directions within the layer plane. The average size of these regions is ca. 50 Å as is indicated by the polarized neutron diffraction profiles. This description of the onset of the magnetic structure may also explain the small maximum in the correlation length that may be present at 20 K in the polarized neutron diffraction measurements on $(d_{20}\text{-}PPh_4)[Fe_2(ox)_3]$. When the compound is heated from its frozen spin structure, the smaller spin correlated regions are more likely to lose their correlations first and, as a consequence, the average observed correlation length increases between 10 and 20 K. Above 20 K the larger exchange correlated domains begin to lose their correlation because of thermal agitation and the correlation length again decreases. Finally, it is interesting to note that a magnetic transition at 16.3 K has been observed[34] in the heat capacity of $(NBu_4)[Fe_2(ox)_3]$ and the proximity of the temperatures of 16.3 and 20 K may indicate that these magnetic transitions have the same origin.

V. CONCLUSIONS

Neutron polarization analysis and Mössbauer spectroscopy have been used to study the short-range antiferromagnetic correlations in the layered insulators (PPh_4) $[Fe^{II}Fe^{III}(ox)_3]$ and (NBu_4) $[Fe^{II}Fe^{III}(ox)_3]$. The absence of magnetic Bragg scattering in the polarized neutron diffraction profiles obtained between 2 and 50 K on $(d_{20}\text{-}PPh_4)$ $[Fe^{II}Fe^{III}(ox)_3]$ indicates the absence of long-range magnetic order. However, a broad asymmetric feature observed at a Q of ca. 0.8 $Å^{-1}$ is attributed to two-dimensional short-range magnetic correlations, which are described by a Warren function. The correlation length is ca. 50 Å between 2 and 30 K and then decreases to ca. 20 Å at 50 K. The Mössbauer spectra of (PPh_4) $[Fe^{II}Fe^{III}(ox)_3]$ and (NBu_4) $[Fe^{II}Fe^{III}(ox)_3]$ have been measured between 1.9 and 293 K and 1.9 and 315 K, respectively, and are very similar. Between 10 and 30 K, paramagnetic scattering in the polarized neutron diffraction profiles of (PPh_4) $[Fe^{II}Fe^{III}(ox)_3]$ and the coexistence of broad sextets and doublets in the Mössbauer spectra both indicate the coexistence of spin-correlated and spin-uncorrelated regions in the layers of this compound on the time scales of both techniques. The polarized neutron scattering profiles yield the spatial correlation length, while the Mössbauer spectra yield the time autocorrelation function, and the combined results are best understood in terms of layers composed of random frozen, but exchange-correlated domains, of ca. 50 Å diameter at the lowest temperatures, of spin-correlated domains and spin-uncorrelated regions at intermediate temperatures, and of largely spin-uncorrelated regions above the apparent Néel temperature as determined from bulk magnetometry. The similarity of the Mössbauer spectra of (PPh_4) $[Fe^{II}Fe^{III}(ox)_3]$ and (NBu_4) $[Fe^{II}Fe^{III}(ox)_3]$ leads us to conclude that similar processes occur in the both compounds.

ACKNOWLEDGMENTS

The authors thank Dr. H. Spiering for useful discussions and ideas during the course of this work and Dr. J. R. Stuart and Dr. K. H. Andersen for valuable assistance with the neutron scattering experiments. G.J.L. thanks the National Science Foundation for Grant No. DMR-9521739 and the Belgian ''Fonds National de la Recherche Scientifique'' for support during a sabbatical leave. This work is supported by the UK EPSRC and EC TMR network ''Molecular Magnets.'' Thanks are due to the Institut Laue-Langevin, Grenoble, for access to neutron facilities.

[1] H. Tamaki, M. Mitsumi, K. Nakamura, N. Matsumoto, S. Kida, H. Okawa, and S. Iijima, Chem. Lett. **1992**, 1975 (1992).
[2] H. Tamaki, Z. Zhong, N. Matsumoto, S. Kida, M. Koikawa, N. Aihiwa, Y. Hashimoto, and H. Okawa, J. Am. Chem. Soc. **114**, 6974 (1992).
[3] S. Iijima, T. Katsura, H. Tamaki, M. Mitsumi, N. Matsumoto, and H. Okawa, Mol. Cryst. Liq. Cryst. Sci. Technol., Sect. A **233**, 263 (1993).
[4] C. Mathonière, S. G. Carling, Y. Dou, and P. Day, J. Chem. Soc. Chem. Commun. **1994**, 1554.
[5] W. M. Reiff, J. Kreisz, L. Meda, and R. U. Kirss, Mol. Cryst. Liq. Cryst. Sci. Technol., Sect. A **273**, 181 (1995).
[6] C. Mathonière, C. J. Nuttall, S. G. Carling, and P. Day, Inorg. Chem. **35**, 1201 (1996).
[7] L. Néel, Ann. Phys. (Paris) **3**, 137 (1948).
[8] I. D. Watts, S. G. Carling, and P. Day, Phys. Chem. Chem. Phys. **3**, 4418 (2001).
[9] C. J. Nuttall and P. Day, Inorg. Chem. **37**, 3885 (1998).
[10] D. Visser, S. G. Carling, I. D. Watts, P. Day, and K. H. Andersen, Physica B **268**, 266 (1999).
[11] H. Okawa, N. Matsumoto, H. Tamaki, and M. Ohba, Mol. Cryst. Liq. Cryst. Sci. Technol., Sect. A **233**, 257 (1993).
[12] S. Iijima, F. Mizutani, M. Mitsumi, N. Matsumoto, and H. Okawa, Inorg. Chim. Acta **253**, 47 (1996).
[13] S. Iijima and F. Mizutani, Mol. Cryst. Liq. Cryst. Sci. Technol., Sect. A **306**, 227 (1997).
[14] S. Iijima and F. Mizutani, Mol. Cryst. Liq. Cryst. Sci. Technol., Sect. A **335**, 143 (1999).
[15] S. Iijima and F. Mizutani, Mol. Cryst. Liq. Cryst. Sci. Technol., Sect. A **343**, 199 (2000).
[16] N. S. Ovanesyan, G. V. Shilov, L. O. Atovmyan, R. N. Lyubovskaya, A. A. Pyalling, and Y. G. Morozov, Mol. Cryst. Liq. Cryst. Sci. Technol., Sect. A **273**, 175 (1995).
[17] N. S. Ovanesyan, G. V. Shilov, N. A. Sanina, A. A. Pyalling, L. O. Atovmyan, and L. Bottyán, Mol. Cryst. Liq. Cryst. Sci. Technol., Sect. A **335**, 91 (1999).
[18] L. Bottyán, L. Kiss, N. S. Ovanesyan, A. A. Pyalling, N. A. Sanina, and A. B. Kashuba, JETP Lett. **70**, 697 (1999).
[19] E. Coronado, J. R. Galán-Mascarós, C. J. Gómez-García, J. Ensling, and P. Gütlich, Chem.-Eur. J. **6**, 552 (2000).
[20] C. J. Nuttall, Ph.D. thesis, University of London, 1998.
[21] I. D. Watts, Ph.D. thesis, University of London, 2000.
[22] O. Schärpf and H. Capellmann, Phys. Status Solidi A **135**, 359 (1993).
[23] C. J. Nuttall and P. Day, Chem. Mater. **10**, 3050 (1998).
[24] P. J. Brown, in *International Tables for Crystallography*, edited by A. J. C. Wilson (Kluwer Academic, Dordrecht, 1999), Vol. C, p. 450.
[25] J. E. Greedan, M. Bieringer, J. F. Britten, G. M. Giaquinta, and H. C. Zurloye, J. Solid State Chem. **116**, 118 (1995).
[26] B. E. Warren, Phys. Rev. **59**, 693 (1941).
[27] J. Fenger, K. E. Siekierska, and A. G. Maddock, J. Chem. Soc. A **1970**, 1456.
[28] M. J. Halsey and A. M. Pritchard, J. Chem. Soc. A **1968**, 2878.
[29] H. Sato and T. Tominaga, Bull. Chem. Soc. Jpn. **52**, 1402 (1979).
[30] R. Ingalls, Phys. Rev. **133**, A787 (1964).
[31] G. J. Long and F. Grandjean, in *Supermagnets, Hard Magnetic Materials*, edited by G. J. Long and F. Grandjean (Kluwer Academic, Dordrecht, 1991) p. 355.
[32] T. E. Cranshaw and G. Longworth, in *Mössbauer Spectroscopy Applied to Inorganic Chemistry*, edited by G. J. Long (Plenum, New York, 1984), Vol. 1, p. 171.
[33] M. F. Thomas and C. E. Johnson, in *Mössbauer Spectroscopy*, edited by D. P. E. Dickson and F. J. Berry (Cambridge University Press, Cambridge, England, 1986), p. 143.
[34] A. Bhattacharjee, Y. Miyazaki, and M. Sorai, J. Phys. Soc. Jpn. **69**, 479 (2000).
[35] A. Bhattacharjee, K. Saito, and M. Sorai, Solid State Commun. **113**, 543 (2000).
[36] A. Bhattacharjee, S. Iijima, F. Mizutani, T. Katsura, N. Matsumoto, and H. Okawa, Jpn. J. Appl. Phys., Part 1 **34**, 1521 (1995).